High-temperature oxidation of FeCrAl alloy with alumina–silica–ceria coatings deposited by sol–gel method

Jacek Chęcmanowski · Aleksandra Matraszek ·
Irena Szczygieł · Bogdan Szczygieł

Abstract One-layer protective coatings made up of SiO_2–Al_2O_3 or SiO_2–Al_2O_3–CeO_2 oxides were synthesized on a FeCrAl alloy substrate by the sol–gel method from sols containing tetraethyl orthosilicate, aluminum tri-*sec*-butoxide and cerium(III) 2,4-pentanedionate as the precursors. Coating solutions with the Si:Al:Ce molar ratio of 3:1:0, 3:1:0.1; 3:1:0.01, and 3:1:0.001 were used. The composition and morphology of the obtained gels were examined by TG/DSC, XRD, and SEM techniques. It was found that a small addition of cerium affected the morphology of the forming coatings and improved the FeCrAl alloy resistance to high-temperature oxidation (in air at $T = 900$ °C for $t = 100$ h). The oxidation of all the investigated samples conformed to the parabolic rate. The protection effectiveness of the one-layer coatings after 100 h of high-temperature oxidation was as high as 70 %.

Keywords Ceramics · SiO_2–Al_2O_3 and SiO_2–Al_2O_3–CeO_2 coatings · High-temperature corrosion · Sol–gel · FeCrAl

Introduction

The resistance of FeCrAl alloys to high-temperature oxidation depends on the properties of the building up

J. Chęcmanowski · B. Szczygieł
Faculty of Chemistry, Wrocław University of Technology,
Wybrzeże Wyspiańskiego 27, 50-370 Wrocław, Poland

A. Matraszek · I. Szczygieł (✉)
Department of Inorganic Chemistry, Institute of Engineering
and Economics, Wrocław University of Economics,
Wrocław, Poland
e-mail: irena.szczygiel@ue.wroc.pl

aluminum oxide. Good protective properties of α-Al_2O_3 (α-alumina) scale stem from its low volatility [1, 2], slow growth rate [2], low concentration of crystalline defects [3], and good chemical stability in high-temperature corrosion environments [4]. But, the scale may crack and spall in the course of cyclic thermal oxidation [5–7].

The protective character of α-Al_2O_3 scale and its adherence to the substrate can be improved through the use of reactive elements (RE), e.g., Zr, Hf, Y, Ce, La, and other rare earth elements) [1, 8–13]. The required RE concentration in the scale depends on several factors such as the chemical composition of the alloy, the amount and kind of impurities (e.g., sulfur) the latter contains, the kind of reactive element and the oxidation conditions (temperature, time, environment). The optimum RE content has been the subject of intensive research conducted in many laboratories [14–22]. According to some authors, the scale acquires the best protective properties in the presence of 10^{-4}–10^{-1} wt% of RE [23]. Others suggest that the optimum RE content is below 0.05 at.% (about 0.3 wt%) [24]. The spallation resistance of the scale is observed to increase already at a Ce content of 0.05 wt% [25]. An excess of Ce may result in the acceleration of the alloy oxidation rate and in the increase in the scale susceptibility to spalling [25–27].

Reactive elements may be introduced into the alloy as alloying elements [16, 17, 19] or in the form of oxides [18, 20, 21]. Also ion implantation is employed for this purpose [28]. Sometimes reactive elements are deposited on the alloy by surface methods, such as sol–gel coating [29–31], MOCVD [32] or electrodeposition [33, 34].

The oxides of reactive elements, e.g., CeO_2, affect the oxidation kinetics of metals [35]. According to the literature reports, when Ce is introduced, the rate of the high-temperature oxidation of alloys considerably decreases [36]. The presence of cerium in the coating and in the scale

contributes to the outward diffusion of cations and to the inward anion transport during oxidation [35–37], eliminates voids in the region near the oxide-substrate interface and improves the adhesion of the scale to the substrate.

Research results indicate that in a temperature range of 1073–1273 K reactive elements affect the phase transformation of transient aluminum oxides of the γ, δ, and θ type to the stable α-Al$_2$O$_3$ phase [38].

The heat resistance of the FeCrAl alloy can be improved by producing vitreous coatings made up of SiO$_2$ and Al$_2$O$_3$ on its surface. As a result of the outward diffusion of Al^{3+} cations and the inward diffusion of oxygen, aluminosilicates (e.g., mullite) form within the coating in the course of high-temperature oxidation [30, 31]. By introducing a reactive element (e.g., Ce) into such a coating one can further increase the heat resistance of the FeCrAl alloy.

FeCrAl-type alloys are designed for operation at temperatures as high as 1400 °C. Sometimes, they are tested and used at temperatures below 1000 °C (for instance as catalytic carriers in cars). In these conditions, α-Al$_2$O$_3$ scale forms much slower and its build-up and protective properties are complicated by the presence of transition aluminas [38].

The aim of the present contribution was to determine the high-temperature resistance of the FeCrAl alloy coated with SiO$_2$–Al$_2$O$_3$ or SiO$_2$–Al$_2$O$_3$–CeO$_2$ (900 °C, under air). The coatings would be obtained by the sol–gel method and deposited using the dip-coating technique. The effect of the cerium content in the coatings on the rate of oxidation of the FeCrAl alloy and on the morphology of the building up Al$_2$O$_3$ scale was determined. Also the thermal behavior of coating materials was described, with special regard to the temperature range in which crystalline phases form and to the effect of powder sintering temperature on the material microstructure. The changes induced by a cerium addition to the aluminosilicate coatings and the contribution of the addition to an improvement in the high-temperature resistance of FeCrAl alloy were studied.

Experimental

Sol preparation

The precursors of: silicon (tetraethyl orthosilicate, Si(OC$_2$H$_5$)$_4$, TEOS), aluminum (aluminum tri-*sec*-butoxide, Al(OC$_4$H$_9$)$_3$, TBA), and cerium (cerium(III) 2,4-pentanedionate, Ce(C$_5$H$_7$O$_2$)$_3$·xH$_2$O, *Ce-acac*) were used to prepare SiO$_2$–Al$_2$O$_3$ and SiO$_2$–Al$_2$O$_3$–CeO$_2$ coating solutions. Each of the precursors would be separately diluted in butyl alcohol (1-butanol, *Bu*-1) and homogenized in an ultrasonic washer for 90 min. A mixture of TEOS and TBA solutions was the base for the SiO$_2$–Al$_2$O$_3$ (sol A) coating solution. Ternary

sols SiO$_2$–Al$_2$O$_3$–CeO$_2$ with a different cerium content (sols B, C, D) were obtained by adding cerium acetylacetonate (III) to sol A. Then, HNO$_3$ (65 %) and CH$_3$COOH (95.5 %) were added to the two kinds (binary and ternary) of sols and homogenized for 120 min. The coating solutions prepared in this way would be aged for 168 h. The composition of the sols is shown in Table 1.

In order to characterize the behavior of the material at high temperature, the A–D sols were gelled in air and the obtained powders were subjected to further thermal treatment.

Samples

The coating substrate material was a ferritic FeCrAl-type alloy (Baildon-Steelplant, Poland) with a chemical composition (wt%): Cr, 18.5; Al, 4.6; Si, 0.81; Mn, 0.6; Ti, 0.01; C, max. 0.05; S, max. 0.07; and Fe as the matrix. The samples were made of 0.06-mm thick foil.

Prior to coating deposition the specimens were ground with abrasive paper (grit no. 400, 600, and 800), degreased in acetone and in distilled water in an ultrasonic bath and dried in a stream of hot air.

SiO$_2$–Al$_2$O$_3$ and SiO$_2$–Al$_2$O$_3$–CeO$_2$ would be deposited on the FeCrAl alloy surface using the dip-coating technique. The sample would be brought to the surface of the solution at a rate of 10 mm min^{-1}. The alloy with the coating would be dried in air for 24 h. Then, the samples would be subjected to preliminary heat treatment under air in a furnace at a temperature of 500 °C for 3 h. The rate of temperature increase in furnace temperature was 2 °C min^{-1}.

Test methodology:high-temperature oxidation

The oxidation of the FeCrAl alloy without and with a SiO$_2$–Al$_2$O$_3$ or SiO$_2$–Al$_2$O$_3$–CeO$_2$ coating was conducted under air at a temperature of 900 °C for 100 h. The alloy resistance to high-temperature oxidation Eq. (1) and the coating's protection effectiveness (S) in comparison with that of the uncoated FeCrAl alloy substrate Eq. (2) were

Table 1 Chemical composition of sols

Sol	A	B	C	D
Si:Al:Ce molar ratio	3:1:0	3:1:0.1	3:1:0.01	3:1:0.001
Alkoxides:alcohol molar ratio	1:4	1:4	1:4	1:4
TEOS/g	6.250	6.250	6.250	6.250
TBA/g	2.463	2.463	2.463	2.463
Ce-acac/g	0.0	0.438	0.044	0.004
Bu-1/g	11.862	12.156	11.889	11.862
HNO$_3$/g	0.050	0.050	0.050	0.050
CH$_3$COOH/g	0.055	0.055	0.055	0.055

determined on the basis of the relative changes in the sample mass versus time:

$$\frac{\Delta m}{m_0} = \frac{m_k - m_0}{m_0} \times 100\ \% \qquad (1)$$

$$S = \frac{\Delta m_0 - \Delta m_p}{\Delta m_0} \times 100\ \% \qquad (2)$$

where m_0, the sample initial mass; m_k, the sample mass after oxidation; Δm_0, the relative gain in the mass of the uncoated FeCrAl alloy; Δm_k, the relative gain in the mass of the coated FeCrAl alloy.

The topography of the SiO_2–Al_2O_3 and SiO_2–Al_2O_3–CeO_2 coatings was examined by scanning electron microscopy (JSM 5800LV made by Joel).

Characterization of powder coating materials

Phase analyses of powder gels A–D were carried out using the XRD technique and a Siemens D5000 diffractometer equipped with a copper radiation cathode. The measurements were performed in a 2θ angle range of 5–50° with a step of 0.04° for at least 3 s per step.

The thermal behavior of the dried gels was determined by combined DSC and TG. The analyses were carried out using the SETSYS^{TM} apparatus (TG-DSC 1500; Setaram). The powdered samples, each weighing 20 mg, were placed in Pt crucibles and heated up to 1200 °C at a heating rate of 10 °C min^{-1} using Ar as the purge gas. The temperature and sensitivity calibration factor for the thermal experiments was determined at the melting points of NaCl (801 °C), $Ca_2P_2O_7$ (1353 °C) and K_2SO_4 (1070 °C) and for the phase transition temperature of the latter compound (583 °C).

Results and discussion

Coating solutions

The obtained SiO_2–Al_2O_3 and SiO_2–Al_2O_3–CeO_2 sols were transparent and monophase. They showed low and constant viscosity (about 4–5 cP; 4–5·10^{-3} Pa s) during no-air access storage for many weeks. The Ce(IV) content affected the sol color. As the Ce(IV) content in the mixture

Fig. 1 Surface of FeCrAl alloy after high-temperature oxidation at 900 °C for 100 h without coating (**a**); with SiO_2–Al_2O_3 layer (**b**); with SiO_2–Al_2O_3–CeO_2 coatings obtained from sol B (**c**); and with SiO_2–Al_2O_3–CeO_2 coatings obtained from sol D (**d**)
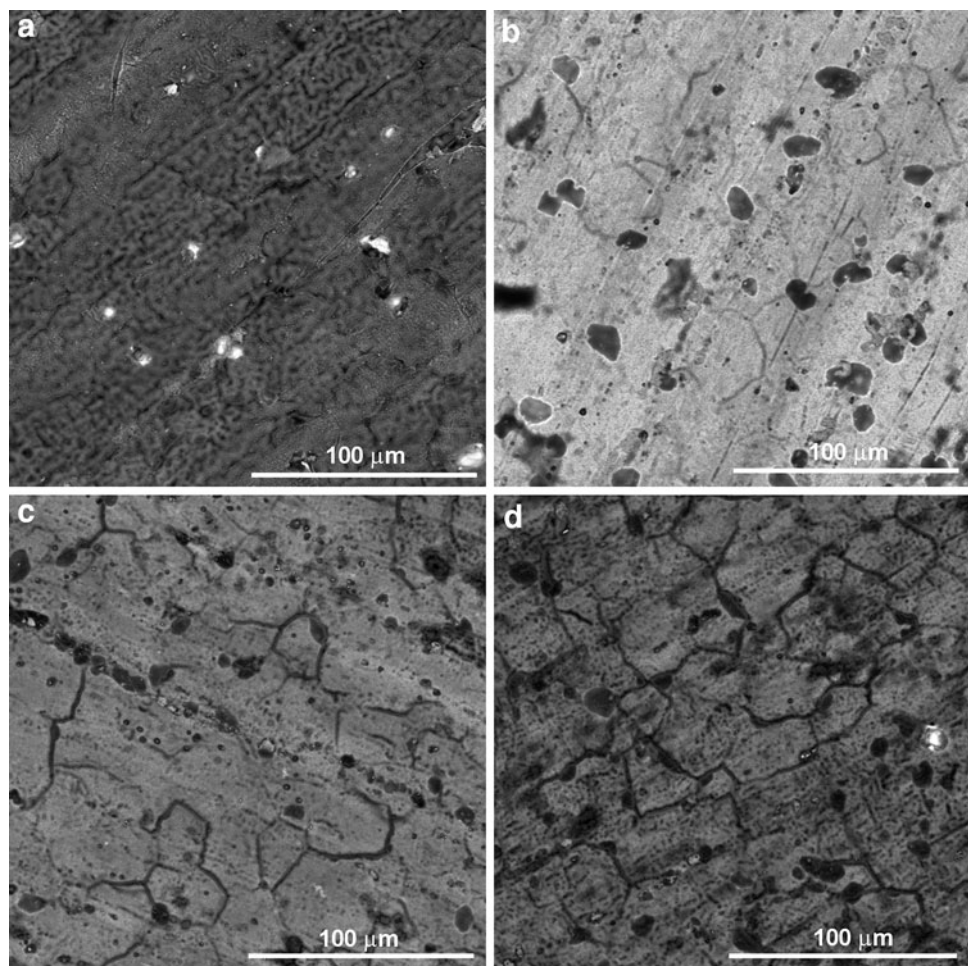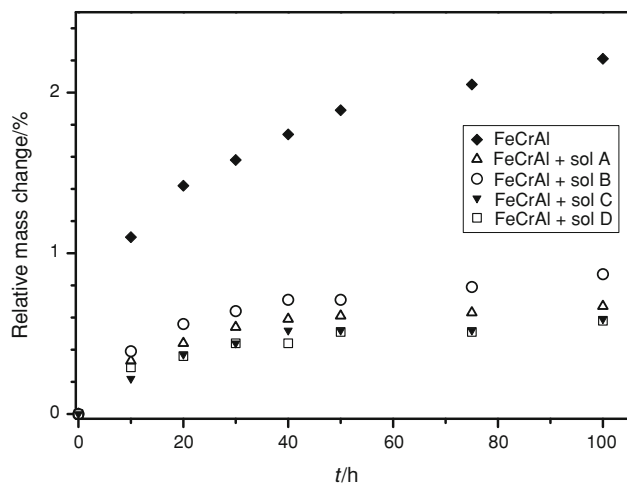
Fig. 2 Relative change in mass of uncoated FeCrAl alloy and alloy covered with $SiO_2–Al_2O_3$ or $SiO_2–Al_2O_3–CeO_2$ coating after oxidation under air at 900 °C

increased, the yellow color of the solution intensified. The quick gelation of the sols on the alloy surface, and so the formation of $SiO_2–Al_2O_3$ and $SiO_2–Al_2O_3–CeO_2$ coatings, was the result of the hydrolysis of the precursors with moisture (water) contained in the air [30, 31, 39, 40].

Morphology of FeCrAl alloy surface after high-temperature oxidation

SEM examinations show a close similarity between the topographies of all the FeCrAl samples after high-temperature oxidation at 900 °C for 100 h (Fig. 1). This applies to both the alloy alone and the alloy covered with two- and three-component oxide coatings. The scale is cracked to a different degree. The fewest cracks occur on the FeCrAl alloy while the most cracks occur on the alloy covered with the ternary $SiO_2–Al_2O_3–CeO_2$ coating. Also the largest number of segregations occur on the alloy with the latter coating. From an analysis of the literature on the subject, it appears that this may be the θ-Al_2O_3 phase [1, 41–48], and the previous studies [30, 31, 49] by the authors indicate the γ-Al_2O_3 form.

Table 2 Protection effectiveness of coatings in comparison with uncoated FeCrAl substrate

Coating	Protection effectiveness/%						
	Oxidation time/h						
	10	20	30	40	50	75	100
A	70.0	69.0	65.8	66.1	67.7	69.3	69.7
B	64.5	60.6	59.5	59.2	62.4	61.5	60.6
C	86.0	73.9	72.2	70.1	72.5	74.6	73.3
D	73.6	74.6	72.2	74.7	73.0	75.1	73.8

Oxidation of FeCrAl alloy and alloy with $SiO_2–Al_2O_3$ or $SiO_2–Al_2O_3–CeO_2$ coating at 900 °C

The samples made of FeCrAl alloy foil without and with a $SiO_2–Al_2O_3$ or $SiO_2–Al_2O_3–CeO_2$ coating do not deform during isothermal high-temperature oxidation. This indicates that the stresses arising at the substrate-scale-coating interfaces are not too high.

In order to determine the behavior of the FeCrAl alloy and that of the latter alloy with sol–gel coatings during oxidation at 900 °C the change in mass as function of time was measured (Fig. 2).

The samples gain in mass is in accordance with the parabolic oxidation rate. The deposition of the vitreous coatings on the alloy results in a reduction in the rate of oxidation of the substrate. It can be assumed that the coatings act as barriers.

The uncoated alloy showed the largest mass increment and so the lowest resistance to oxidation. The $SiO_2–Al_2O_3$ sol–gel coating clearly improves the behavior of the samples. In the case of the three-component coatings with CeO_2, the mass increment depends on the cerium content. The presence of a large amount of cerium (sol B, Si:Al:Ce = 3:1:0.1) results in a deterioration in oxidation resistance in comparison with the alloy covered with the $SiO_2–Al_2O_3$ coating. This has also been observed for other reactive elements by other researchers [1–4, 7–17, 19, 20, 25–29]. A small amount of cerium in the coating (sols C and D, Si:Al:Ce = 3:1:0.01 and 3:1:0.001) reduces the rate of oxidation
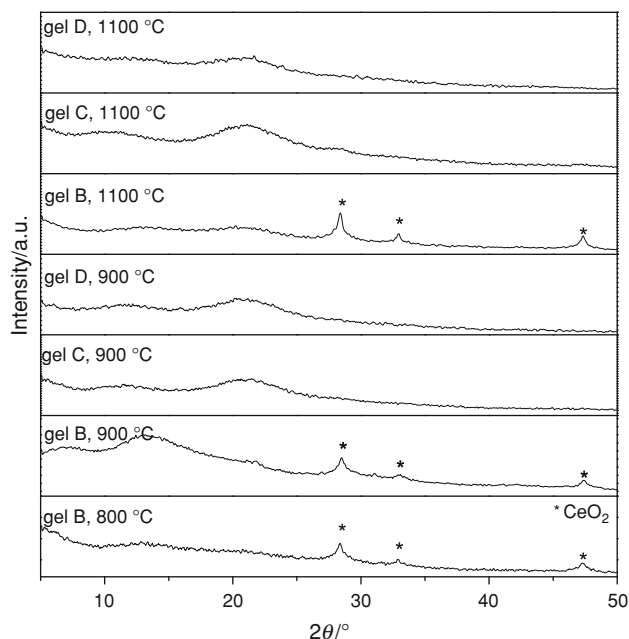

Fig. 3 The XRD patterns of coating materials sintered at different temperatures
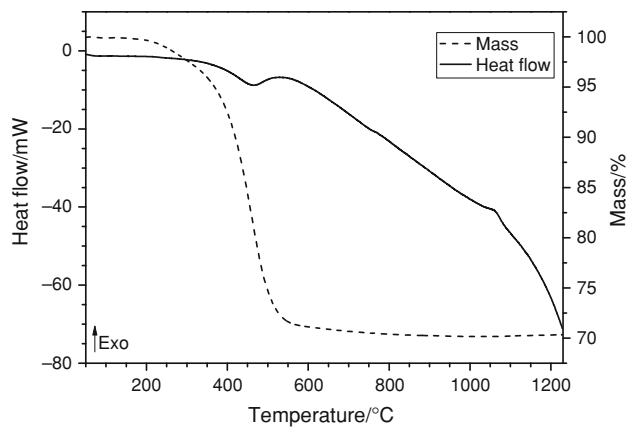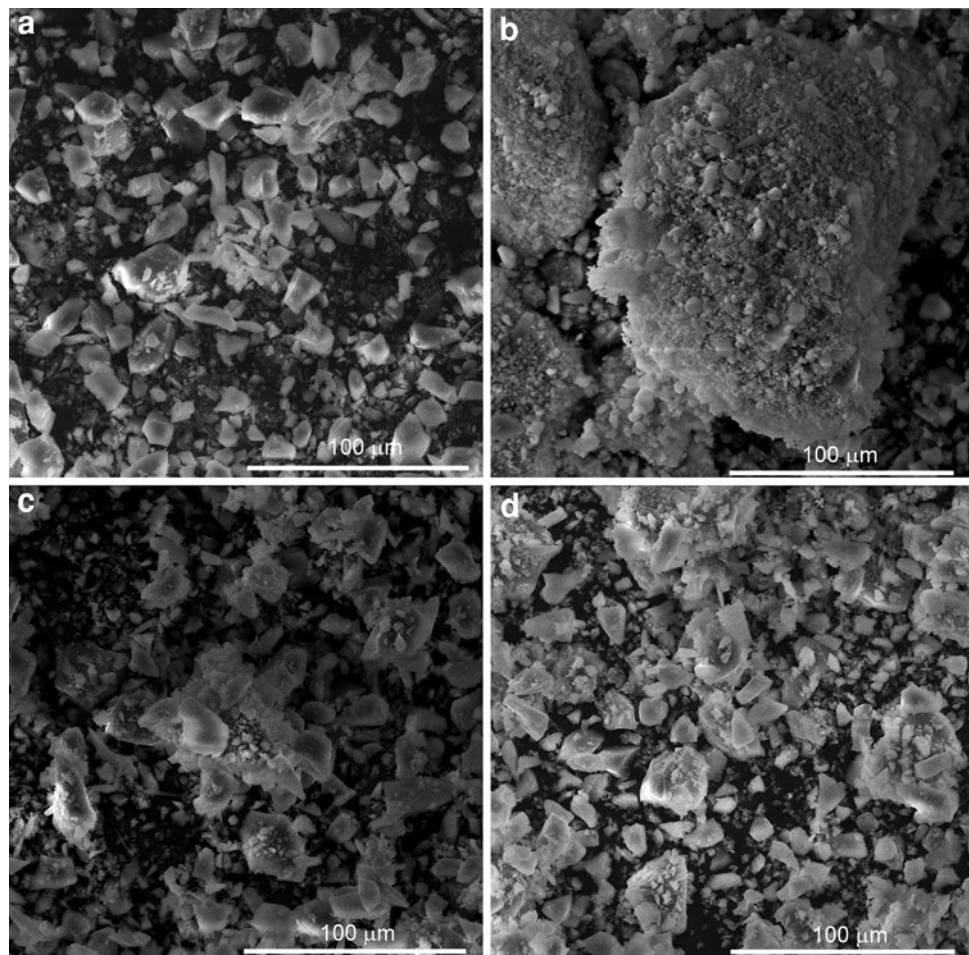
Fig. 4 The DSC/TG curves of heating of gel C

of the alloy, also in comparison with the sample covered with the SiO_2–Al_2O_3 (sol A) coating.

The protection effectiveness of the coatings during high-temperature oxidation ranges from 60 to 74 % (Table 2) and remains at a constant level over time (100 h), which indicates their high stability.

Characterization of coating materials

The phase composition of the gelled and sintered coating materials was determined by the XRD method. The materials are rich in silica (86 mol% SiO_2; 14 mol% Al_2O_3) and their composition corresponds to the spinodal region in the binary SiO_2–Al_2O_3 system in a wide temperature range ($\sim$700–1250 °C) [50]. The XRD patterns of the samples subjected to thermal treatment at 800 °C (5 h), 900 °C (100 h), and 1100 °C (10 h) are shown in Fig. 3. An analysis of the XRD patterns of the sols dried at room temperature and then annealed at 500° for 3 h showed their noncrystalline character. Also the samples with a low Ce content (sols C and D) had an amorphous character. Whereas the thermal treatment of sample B resulted in the crystallization of cerium oxide. The presence of crystalline CeO_2 in samples C and D was not confirmed by the XRD method—probably due to the low cerium oxide content in the gels (the amount undetectable by XRD method).

The powdered gels were analyzed by the DSC/TG methods. As an example, Fig. 4 shows the heating curve for gel C. The shape of the DSC and TG curves for the

Fig. 5 Morphology of SiO_2–Al_2O_3 and SiO_2–Al_2O_3–CeO_2 gels after heat treatment at 900 °C for 100 h obtained from sol A (**a**), sol B (**b**), sol C (**c**), and sol D (**d**)

other samples is similar. In a temperature range up to about 550° a single-step decrement (amounting to 28–30 wt%.) in the mass of the preparation was registered on the TG curves for the samples. This decrement was accompanied by an endothermic thermal effect on the DSC curves, with a maximum at a temperature of 500, 460, and 420 °C for, respectively, sol B, C, and D. The mass decrement registered in this range of temperatures can be ascribed to the dehydration of the gel and to the decomposition of its components (alcoholates).

At a temperature of 1060 °C, a weak exothermic effect was observed on the DSC curves. Unfortunately, an analysis of the XRD samples sintered at 1100 °C (Fig. 3) did not confirm the presence of a new crystalline phase, probably due to the XRD method low sensitivity in detecting small amounts of phases. However, the available literature data indicate that the registered exothermic effect can be ascribed to the crystallization of the original mullite or crystobalite [51–54].

Morphology of powders obtained from A to D sols after sintering at 900 °C

The morphology of the powders obtained from sols A to D after sintering at 900 °C for 100 h varies (Fig. 5). The SiO_2–Al_2O_3 grains obtained from sol A have an irregular shape, a smooth surface (Fig. 5a and characteristics of the vitrified phase. As the cerium oxide content in the material increases, the powder grains become smaller and agglomerate to a considerable degree and the percentage of the fraction characterized by smooth surface decreases (Fig. 5b–d). At the same time, crystalline cerium oxide was found to be present only in the preparation obtained from sol B (with the highest CeO_2 content) (Fig. 3). The other powders (gels A, C and D) had an amorphous character. The authors' earlier studies [50] on the effect of the thermal treatment of aluminosilicate gels (with different Si:Al molar ratios) on their morphology showed that an increase in the amount of the crystalline fraction in the preparations results in an increase in the specific surface area of the powders, and thus in an increase in their porosity. These are undesirable effects if such materials are to be used for coatings which are to protect alloys against high-temperature corrosion.

Conclusions

On the basis of the results of the studies one can conclude that

(1) Single-layer protective SiO_2–Al_2O_3 or SiO_2–Al_2O_3–CeO_2 coatings obtained by the sol–gel method and

deposited on the FeCrAl alloy using the dip-coating technique improve the substrate resistance to high-temperature oxidation. The presence of ternary coatings on the metallic substrate results in different gains in the mass of the alloy depending on the cerium oxide content. Because of the higher cerium content in the coating obtained from sol B (Si:Al:Ce = 3:1:0.1), the sample resistance is worse than that of the alloy with coating A (SiO_2–Al_2O_3) and with coatings C–D. As the amount of cerium in the coating decreases (sols C–D with Si:Al:Ce molar ratios of respectively 3:1:0.01 and 3:1:0.001), the rate of oxidation of the alloy relative to that of the alloy covered with the SiO_2–Al_2O_3 coating also decreases.

(2) The samples gain in mass is in accordance with the parabolic oxidation rate. The fact that the samples (in the form of thin foils) do not undergo deformation when subjected to high-temperature oxidation indicates that the stresses arising at the substrate-scale-coating interfaces are not too high.

(3) The protection effectiveness of the coatings ranges from 60 to 74 % in the course of 100 h of high-temperature oxidation.

(4) During high-temperature oxidation at 900 °C characteristic segregations form on the surface of the FeCrAl alloy. The largest number of such segregations occur on the alloy covered with the three-component SiO_2–Al_2O_3–CeO_2 coating. The segregations may constitute a θ-Al_2O_3 or γ-Al_2O_3 phase.

(5) The fraction of a crystalline phase (CeO_2) in the powders obtained from the sols through sintering at 900 °C affects the morphology of the powders. As the amount of cerium oxide in the material increases, the powder grain size decreases considerably whereby the material specific surface increases. The increase in the surface development of the powders may be responsible for the worse protective properties of the coatings produced from the three-component sols with the highest CeO_2 content.

References

1. Nguyen CT, Buscail H, Cueff R, Issartel C, Riffard F, Perrier S, Poble O. The effect of cerium oxide argon-annealed coatings on the high temperature oxidation of a FeCrAl alloy. Appl Surf Sci. 2009;255:9480–6.

2. Golightly FA, Wood GC, Stott FH. The early stages of development of alpha-Al$_2$O$_3$ on Fe–Cr–Al and Fe–Cr–Al–Y alloys at high temperature. Oxid Met. 1980;14:217–34.

3. Biegun T, Danielewski M, Skrzypek Z. The reactive element effect in the high temperature oxidation of Fe–23Cr–5Al commercial alloys. Oxid Met. 1992;38:207–15.

4. Pint BA, Martin JR, Hobbs LW. The reactive element effect in commercial ODS FeCrAl alloys. Solid State Ionics. 1995;78:99–107.

5. Stott FH, Wood GC. Growth and adhesion of oxide scales on Al$_2$O$_3$-forming alloys and coatings. Mater Sci Eng. 1987;87:267–74.

6. Tolpygo VK. Segregation at Al$_2$O$_3$–FeCrAl interface during high temperature oxidation. Oxid Met. 1999;51:449–74.

7. Pint BA, Garratt-Reed AJ, Hobbs LW. The reactive element effect in commercial ODS FeCrAl alloys. Mater High Temp. 1995;13(1):3–15.

8. Amano T. Rare earth application for heat-resisting alloys. J Rare Earths. 2010;28:12–21.

9. Amano T, Isobe I, Sakai N, Shishido T. The effects of yttrium addition on high-temperature oxidation of heat-resistant alloy with sulfur. J Alloys Comp. 2002;344:394–400.

10. Fukuda K, Takao K, Hoshi T, Usui Y, Furuki O. Improvement of high temperature oxidation resistance of rare earth metaladded Fe–20 %Cr–5 %Al alloys by pre-annealing treatment. Mater High Temp. 2003;20:319–26.

11. Pint BA, More KL, Wright IG. The use of two reactive elements to optimize oxidation performance of alumina-forming alloys. Mater High Temp. 2003;20:375–86.

12. Amano T, Isobe H, Yamada K, Shishido T. The morphology of alumina scales formed on Fe–20Cr–4Al–S alloys with reactive element (Y, Hf) additions at 1273 K. Mater High Temp. 2003;20:387–93.

13. Kochubey V, Al-Badairy H, Tatlock G, Coze J Le, Naumenko D, Quadakkers WJ. Effects of minor additions and impurities on oxidation behavior of FeCrAl alloys. development of novel surface coatings compositions. Mater Corros. 2005;56:848–53.

14. Mennicke C, Schumann E, Ruhle M, Hussey RJ, Sproule GI, Graham MJ. The effect of yttrium on the growth process and microstructure of a-Al$_2$O$_3$ on FeCrAl. Oxid Met. 1998;49:455–66.

15. Wolff IM, Iorio LE, Rumpf T, Scheers PVT, Potgieter JH. Oxidation and corrosion behaviour of Fe–Cr and Fe–Cr–Al alloys with minor alloying additions. Mater Sci Eng A. 1998;241:264–76.

16. Moon DP, Bennett MJ. The effect of reactive elements on oxide coating on the oxidation behaviour of metals and alloys at high temperature. Mater Sci Forum. 1989;43:269–89.

17. Hou PY, Shui ZR, Chuang GY, Stringer J. Effect of reactive element oxide coatings on the high temperature oxidation behavior of a FeCrAl alloy. J Electrochem Soc. 1992;139:1119–26.

18. Czyrska-Filemonowicz A, Clemens D, Quadakkers WJ. The effect of high temperature exposure on the structure and oxidation behaviour of mechanically alloyed ferritic ODS alloys. J Mater Process Technol. 1995;53:93–100.

19. Ishii K, Taniguchi S. Effect of La and Hf additions on the high-temperature oxidation resistance of high-purity Fe–20Cr–5Al alloy foils. Oxid Met. 2000;54:491–508.

20. Merceron G, Molins R, Strudel JL. Oxidation behaviour and microstructure evolution of FeCrAl ODS alloys at high temperature. Mater High Temp. 2000;17:149–57.

21. Tyagi AK, Szot K, Czyrska-Filemonowicz A, Naumenko D, Quadakkers WJ. Significance of crystallographic grain orientation for oxide scale formation on FeCrAl ODS alloys studied by AFM and MCS + -SIMS. Mater High Temp. 2000;17:159–63.

22. Chevalier S, Strehl G, Buscail H, Borchardt G, Larpin JP. Influence of the mode of introduction of a reactive element on the high temperature oxidation behavior of an alumina-forming alloy. Part II. cyclic oxidation tests. Mater Corros. 2004;55(8):610–6.

23. Czyrska-Filemonowicz A, Szot K, Wasilkowska A, Gil A, Quadakkers WJ. Microscopy (AFM, TEM, SEM) studies of oxide scale formation on FeCrAl based ODS alloys. Solid State Ionics. 1999;117:13–20.

24. Unocic KA, Parish CM, Pint BA. Characterization of the alumina scale formed on coated and uncoated doped superalloys. Surf Coat Technol. 2011;206:1522–8.

25. Shao M, Cui L, Zheng Y, Xing L. Effect of cerium addition on oxidation behavior of 25Cr20Ni alloy under low oxygen partial pressure. J Rare Earths. 2012;30(2):164–9.

26. Jin HM, Liu XJ, Zhang LN. Influence of nanometric ceria coating on oxidation behavior of chromium at 900 °C. J Rare Earths. 2007;25(1):63–7.

27. Brylewski T, Dąbek J, Przybylski K. Oxidation kinetics study of the iron-based steel for solid oxide fuel cell application. J Therm Anal Calorim. 2004;77(1):207–16.

28. Cueff R, Buscail H, Caudron E, Issartel C, Riffard F. Oxidation of alumina formers at 1173 K: effect of yttrium ion implantation and yttrium alloying addition. Corros Sci. 2003;45:1815–31.

29. Ramanathan LV, Pillis MF, Fernandes SMC. Role of rare earth oxide coatings on oxidation resistance of chromia-forming alloys. J Mater Sci. 2008;43(2):530–5.

30. Chęcmanowski JG, Szczygieł B, Tylus W, Szczygieł I. High-temperature oxidation resistance of FeCrAl alloys coated with silica-rich ceramic SiO$_2$–Al$_2$O$_3$ deposited by sol–gel method. Mater Chem Phys. 2011;126:409–16.

31. Chęcmanowski JG, Szczygieł B. High temperature oxidation resistance of FeCrAl alloys covered with ceramic SiO$_2$–Al$_2$O$_3$ coatings deposited by sol–gel method. Corros Sci. 2008;50:3581–9.

32. Houngniou C, Chevalier S, Larpin JP. High-temperature-oxidation behavior of iron–aluminide diffusion coatings. Oxid Met. 2006;65:409–39.

33. Lu X, Zhu R, He Y. Reactive element effect of electrodeposited Y$_2$O$_3$ Oxide films on the oxidation of Fe–25Cr and Fe–25Cr–10Al alloys. Oxid Met. 1995;43:217–36.

34. Jung HG, Kim KY. Effect of yttrium coating on the oxidation behavior of Ni$_3$Al. Oxid Met. 1996;46:147–67.

35. Peng X, Guan Y, Dong Z, Xu C, Wang F. A fundamental aspect of the growth process of alumina scale on a metal with dispersion of CeO$_2$ nanoparticles. Corros Sci. 2011;53:1954–9.

36. Yu X, Sun Y. The oxidation improvement of Fe$_3$Al based alloy with cerium addition at temperature above 1000 °C. Mater Sci Eng A. 2003;363:30–9.

37. Sundararajan T, Kuroda S, Kawakita J, Seal S. High temperature corrosion of nanoceria coated 9Cr–1Mo ferritic steel in air and steam. Surf Coat Technol. 2006;201:2124–30.

38. Cueff R, Buscail H, Caudron E, Issartel C, Riffard F. Oxidation behaviour of Kanthal A1 and Kanthal AF at 1173 K: effect of yttrium alloying addition. Appl Surf Sci. 2003;207:246–54.

39. Chęcmanowski JG, Szczygieł B. Effect of nanosilica type on protective properties of composite ceramic coatings deposited on steel 316L by sol–gel technique. J Non-Cryst Solids. 2008;354:1786–95.

40. Conde AR, Giampaolo Di, Puerta M, Ruiz H, Olivares JL. Thick aluminosilicate coatings on carbon steel via sol–gel. J Non-Cryst Solids. 1992;147–148:467–73.

41. Amano T, Takezawa Y, Shiino A, Shishido T. Surface morphology of scale on FeCrAl (Pd, Pt, Y) alloys. J Alloys Comp. 2008;452:16–22.

42. Jia L, Shen M, Wang J. Preparation and characterization of dip-coated γ-alumina based ceramic materials on FeCrAl foils. Surf Coat Technol. 2007;201:7159–65.

43. Tolpygo VK, Clarke DR. Microstructural study of the theta-alpha transformation in alumina scales formed on nickel–aluminides. Mater High Temp. 2000;17:59–70.

44. Chevalier S, Nivot C, Larpin JP. Influence of reactive element oxide coatings on the high temperature oxidation behavior of alumina-forming alloys. Oxid Met. 2004;61:195–217.

45. Blachere JR, Schumann E, Meier GH, Pettit FS. Textures of alumina scales on FeCrAl alloys. Scrip Mater. 2003;49:909–12.

46. Wessel E, Kochubey V, Naumenko D, Niewolak L, Singheiser L, Quadakkers WJ. Effect of Zr addition on the microstructure of the alumina scales on FeCrAlY-alloys. Scrip Mater. 2004;51:987–92.

47. Dryepondt S, Pint BA, Lara-Curzio E. Creep behavior of commercial FeCrAl foils: beneficial and detrimental effects of oxidation. Mater Sci Eng A. 2012;550:10–8.

48. Montealegre MA, Strehl G, Gonzalez-Carrasco JL, Borchardt G. Oxidation behaviour of novel ODS FeAlCr intermetallic alloys. Intermetallics. 2005;13:896–906.

49. Silva RS, Macedo ZS. Al_2O_3-based pigments synthesized by a new proteic sol–gel method. J Therm Anal Calorim. 2011;103:587–90.

50. Jantzen CM, Schwahn D, Schelten J, Herman H. The SiO_2–Al_2O_3 system part I. later stage spinodal decomposition and metastable immiscibility. Phys Chem Glasses. 1981;22:122–37.

51. Szczygieł I, Matraszek A, Chęcmanowski J, Szczygieł B. Thermal behaviour of mixed alumina–silica gels obtained from alkoxides: phase formation and morphology of powders. J Non-Cryst Solids. 2010;356:2824–30.

52. Okada K, Otsuka N. Formation process of mullite. In: Somiya S, Davis RF, Pask JA, editors. Mullite and mullite matrix composites, ceramic transitions. Westerville: American Ceramic Soc; 1990. p. 375–87.

53. Risbud SH, Draper VF, Pask JA. Dependence of phase composition on nuclei available in SiO_2–Al_2O_3 mixtures. J Am Ceram Soc. 1978;61:471–2.

54. Avdin VV, Krivtsov IV, Dyachuk VV, Zherebtsov DA. Thermal Behavior of the composite xerogels of zirconium oxyhydroxide and silicic acid. J Therm Anal Calorim. 2012;109:1261–5.